Partial Discharge Detection and Diagnosis of Transformer Bushing Based on UHF Method

Jun Jiang, *Senior Member*, *IEEE*, Judong Chen, Jiansheng Li, Xiaoping Yang, Yifan Bie, Prem Ranjan, Chaohai Zhang, Harald Schwarz

***Abstract*—Bushings are essential components in a power transformer where incipient partial discharge (PD) activities and its detection and diagnosis cannot be ignorant. In this paper, an oil-impregnated paper (OIP) bushing is modeled to investigate that the oil gaps between the flange and condenser body in a typical OIP bushing provide a feasible path to trace the electromagnetic signal. As a non-destructive method, UHF (Ultra High Frequency) is proposed to detect 4 typical inside and outside PD defects of 110 kV bushings. To analyze the parameters of different defects, not only phase-resolved partial discharge (PRPD) is presented, but also 16 detailed time-domain and frequency-domain parameters of UHF signal are involved. Then feature extraction and selection are conducted through comparative principal component analysis (PCA) and extremely randomized trees (ET) algorithms. It is revealed that the selected features are representative and ET greatly reduces the amount of data whilst ensuring high accuracy. Fault diagnosis for bushing is finally achieved via support vector machine (SVM) with the selected features. The presented work of bushing PD detection based on UHF sensors provides a complete solution for the bushing diagnosis in potential field application and maintenance.**

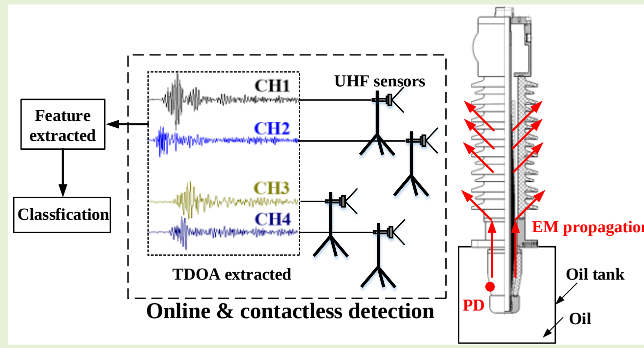

***Index Terms*—Ultra High Frequency; Bushing; Partial Discharge; Principal Component Analysis; Extremely Randomized Trees**

I. Introduction

TRANSFORMER bushing is one of the most important components of a large scale electric power transformer, providing insulation between conductors and transformer tanks. Based on the field experience, oil leakages, insulation deterioration and mechanical damages are attributed as the main root causes of failures [1]. According to latest CIGRE reports, bushings involves 5 to 50 % of the transformer failures, often followed by transformer damages, explosions even fires, huge collateral damage and unexpected shutdown [2,3]. Therefore, it is significant to monitor the high voltage (HV) bushings of power transformers. However, their working status has been used to be ignored.

There are several conventional methods to determine the healthy state of oil-impregnated paper (OIP) bushing, like measuring bushing insulator capacitance, dissipation factor (tanδ), the relative capacitance and relative dielectric loss, which are sensitive to overall damp and capacitor breakdown in the bushing [4,5]. Since the change in moisture content is more sensitive to frequencies, frequency domain spectroscopy method (FDS) is proposed to get more information about the technical state of bushing insulating system from the degree of its wetness [6-9]. Generally, it expands the frequency of the test voltage from the power frequency to a frequency band ranging 0.001 Hz - 1000 Hz. But the information from FDS is still insufficient as it is based on dielectric dissipation, and also requires transformer unplanned outage [10]. In case of the oil-paper insulation system, decompositions also carry a lot of information and provide another good choice to get an insight of the working status of a bushing. As a widely used technique for decomposition detection, dissolved gases analysis (DGA) is practically effective to evaluate discharging and over-heating faults in oil-immersed equipment like power transformers [11-13], but it is difficult to excrete the oil samples at its take-off valve regularly for the oil-less immersed equipment like

Manuscript received XXXX, 2021. This work is supported by Jiangsu Planned Projects for Postdoctoral Research Funds, Project funded by China Postdoctoral Science Foundation (2019M661828) and the Science and Technology Project of State Grid Corporation of China (No. J2019008). The authors also gratefully acknowledge financial support from 2019 CAST Outstanding International Youths Exchange Program.

Jun Jiang, Yifan Bie, and Chaohai Zhang (*Corresponding Author*) are with the Jiangsu Key Laboratory of New Energy Generation and Power Conversion, Nanjing University of Aeronautics and Astronautics, Nanjing, China, 211106 (e-mail: jiangjun0628@163.com);

Judong Chen is with State Grid Jiangxi Maintenance Company, Jiangxi, 330000, China;

Jiansheng Li is with State Grid Jiangsu Electric Power Co. Ltd. Research Institute, Nanjing, 211103, China;

Xiaoping Yang is with State Grid Jiangsu Electric Power Co. Ltd., Nanjing, 210014, China;

Prem Ranjan is with the Department of Electrical & Electronic Engineering, School of Engineering, The University of Manchester, Manchester M13 9PL, UK (e-mail: ppremranjan@gmail.com);

Harald Schwarz is with Energy Distribution and High Voltage Engineering, Faculty 3, Brandenburg University of Technology Cottbus-Senftenberg, Cottbus 03046, Germany (e-mail: harald.schwarz@b-tu.de).

This article has been accepted for publication in a future issue of this journal, but has not been fully edited. Content may change prior to final publication. Citation information: DOI 10.1109/JSEN.2021.3066809, IEEE Sensors Journal

bushings. Besides, continuous online monitoring such as installing electric sensors on the tap has been proposed, but it would bring hidden safety hazards [14,15]. Another way is by installing pressure sensor on the drain valve, but this method can only detect bubble insulation defects [7]. All of these detection methods impair the bushings condition and reliability, whereas the detection information is not timely, sufficient and effective.

As a matter of fact, electrical field strength in the bushing condenser body is among the highest in high voltage equipment, due to the compact mechanical structure. Defective materials or workmanship could cause uneven electric field distribution and lead to partial discharge (PD) activities at the early stage of a bushing insulation failure [16]. PD means local dielectric overstress or weakness and the spread of discharges could eventually result in punctures within the layer of capacitors and short-circuited conductive foils. To avoid these severe damages, it is important to detect PD-induced dielectric insulation degradation at the very early stage of development. Thus, PD detection for transformer bushing should be paid more attention instead of relying on preventive offline measurements or risky online measurements. In fact, PD detection is widely recognized in high voltage apparatus like power transformer, power cable and gas-insulated switchgear (GIS), etc. [17, 18]. Moreover, it is practical to guideline the maintenance through identifying PD types on the basis of typical PD models, extracting signal features and classifications [19-21]. However, as an auxiliary part of a power transformer, the structure of bushing is quite different from GIS, etc., the existing PD experience and diagnosis is not suitable for bushings since its complicated structure limits the UHF signals propagation. Then, how to detect PD activities occurring in bushings through nondestructive testing and how to evaluate the PD type, are extremely challenging for practical applications.

Since ultra-high frequency (UHF) technique has the advantage in contactless detection for power apparatus without influencing the normal operation of the device [22-24], it could be considered as an effective approach to measure PD occurring in bushings. In this paper, a three-dimensional bushing is established and the propagation route of electromagnetic (EM) signal is verified through calculation firstly. Then, 4 typical bushing PD faults are made and detected in the lab based on nondestructive UHF technique. Afterwards, principal component analysis (PCA) and extremely randomized trees (ET) are implemented and compared for feature selection. At last, support vector machine (SVM) algorithm is optimized to achieve PD type recognition and diagnosis, which is beneficial to bushing and transformer maintenance in real time.

II. SIMULATION OF PD-INDUCED ELECTROMAGNETIC IN OIP BUSHING

Due to compact mechanical design and closed structure of the bushing, catadioptric phenomenon of UHF signal induced by PD inside the bushing makes it uncertain and difficult to be detected outside. Therefore, it is necessary to clarify the path and process of EM signal leaking from bushing inside to outside.

A 3D mechanical software is used to model the bushing according to physical size of BRDW-126/630-4, 110 kV bushing. In the actual 110 kV bushing, the condenser body contains 28 equivalent capacitors in series and each layer is 7 μm thick. To simplify the calculation, the condenser body of the bushing is simplified to 4 layers of capacitors as shown in Fig. 1. In the condenser, the thickness of OIP is set as 1 mm, in accordance with the physical size. As EM signal cannot penetrate metal, it doesn't make any differences to increase the capacitor thickness from 7 μm to 4 mm. Then the simplified model is imported into the EM simulation software to evaluate the propagation process. The finite difference time domain (FDTD) method is used to analyze the propagation process of UHF EM signal.

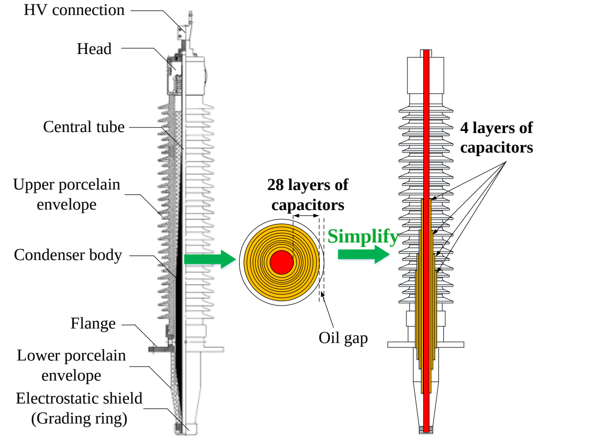

Fig.1 Structure modelling and simplification process of 110 kV bushing

To get an insight of UHF signal propagation, PD is set inside the oil tank below the bushing electrostatic shield. The PD circuit is constructed by a current source in series a 10 Ω resistor. The waveform of the current source is set as Gaussian pulse with the width of 1 ns. Capacitors, flange and central tube are set as perfect electric conductor (PEC), which has a conductivity of infinity. The relative permittivity of porcelain, OIP and oil are 5.8, 3.6 and 2.2 respectively. There are seven layers of perfect matched layer (PML) set at the area boundary to ensure no reflection from the boundary. In the simulation, PML is an artificial absorbing material that absorbs the incident energy as it propagates through the PML layers. The PML layers provide good absorption and seven PML layers are enough to absorb all the signals received. The process of EM signal propagation during 1 ns to 5 ns is shown in Fig. 2.

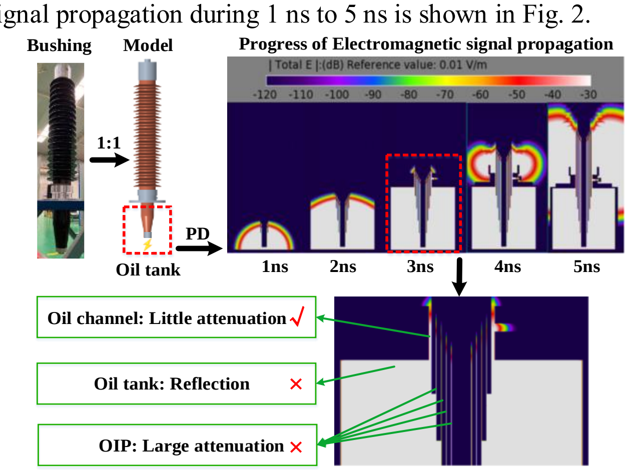

Fig.2 Process of EM signal propagation from oil tank to outside

According to the process of EM signals propagation, at about 2 ns, the oil tank is already filled with EM waves. At 3 ns, it leaks to the outside through OIP and oil gaps (the space between the condenser body and flange) on both sides of the bushing. In an actual bushing, there is a large attenuation of the EM signal due to skin effects of metal, and when it propagates in the OIP, there will be losses due to the dielectric loss. Therefore, the time-dependent propagation of PD-induced EM signal reveals that oil gaps provide an effective path to propagate out with regard to the PD activities inside the oil tank. This calculation indicates that it's feasible to carry out the contactless PD detection based on UHF sensors in theory.

III. TYPICAL PD FAULTS AND TESTING SETUP

To investigate the feasibility of using the UHF method to detect the PD from outside, several real bushings with artificial defects are engaged for the PD test. The OIP bushing used in the experiment is manufactured by Zhida High Voltage Electric Company (China), at its rated voltage of 110 kV. In the HV test circuit, a step-up transformer (150 kV/50 kVA), a coupling capacitor (800 pF) and a bushing connected with bellows, the coupling capacitor is connected in parallel with the bushing to acquire the voltage signal due to PD phenomenon. The substructure bushing is set in the oil tank to imitate the installation on an oil-immersed power transformer. Four UHF sensors are set around the bushing to receive PD-induced EM signals but only two of them are enclosed in Fig.3. The PD level of the laboratory background at 110 kV is smaller than 5 pC, which provides excellent ambient surroundings for the following tests.

Fig.3 Experimental setup and wiring in high voltage laboratory

To get an insight into the PD characteristic in a bushing, 4 typical bushing PD fault types to simulate actual defects are studied in our work, viz.(a) Corona discharge at the top of bushing, (b) Suspension discharge of electrostatic shield, (c) Creeping discharge along the surface of lower porcelain envelope and(d) Interior discharge of the bushing; as shown in Fig.4 and described below.

(a) Corona discharge at the top of bushing. A 5 cm thin metal tip is attached to the surface of upper electrostatic shield on the head and fixed with tape. The electric field strength at the end of tip is extremely high while applying high voltage, the nonuniformity could lead to air ionization and partial discharge. Thereby this type of PD setting simulates PD failures related to rough surface and metal protrusion in real applications.

(b) Suspension discharge of electrostatic shield. This type is aimed to simulate the failure of electrostatic shield falling off but hanging on the wire under actual working conditions. Electrostatic shield is tied up by cloth tape but not in contact with the high voltage part of the bushing. Therefore, suspended discharge appears as it is very closed to the high-voltage part.

(c) Creeping discharge along the surface of lower porcelain envelope. Creeping discharge occurs if the voltage increases when the surface of the lower porcelain envelope is dirty or rough. A hard copper wire is adhered to the surface of the lower porcelain envelope and its end is connected to the electrostatic shield which is under high voltage. The wire head is wrapped with insulating tapes to prevent tip discharge.

(d) Interior discharge of outermost capacitor. As the foils in the condenser body are used to make the electric field uniform, then the uneven edge of foil will result in uneven field distribution. As shown in Fig.4, the bottom of the outermost foil (connected to tap) is artificially made with a jagged fracture. As the electric field strength in the outermost foil is the highest, it easily causes PD while applying high voltage to the bushing. It is set inside the bushing prior to manufacturing, the bottom of the foil is not flat but jagged as many triangles, and the sharp fringe is stressed by the high voltage. Afterwards, the bushing is assembled as usual. It is aimed to simulate the failure of foil fracture under actual working conditions.

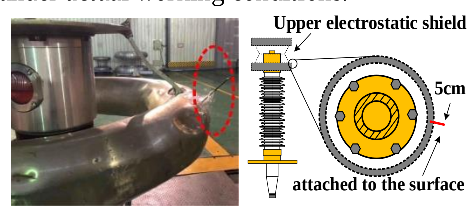

(a) Corona discharge at the top of bushing

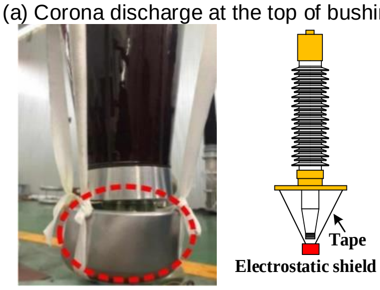

(b) Suspension discharge of electrostatic shield

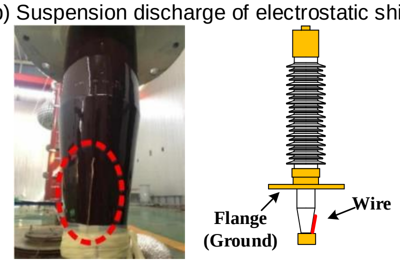

(c) Creeping discharge along the surface of lower porcelain envelope

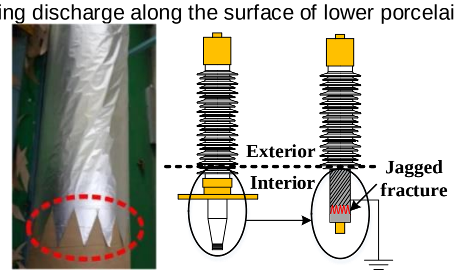

(d) Interior discharge of the bushing

Fig.4 Four different PD faults settings of 110kV OIP bushings

The PD signal of corona discharge is easy to be detected directly outside the bushing. Suspension discharge, creeping discharge are in the oil tank and capacitor discharge is inside the bushing, the UHF signals generated by PD leak from the oil gaps on both sides of the bushing to the external space. Therefore, valid signals can also be detected externally.

Four UHF sensors (ZCCGQ-U-PZ-01) are connected to the signal amplifier module with the gain of 40 dB, whose outputs are then sent to oscilloscope (LeCroy 610Zi) working as a high-speed data acquisition unit. The bandwidth of sensors is 300 MHz - 2 GHz and the matching impedance is 50 Ω. The center of the flange is set as origin and the coordinates of UHF sensors are S1 [3.75 m, 1.68 m, 1.00 m], S2 [1.47 m, 2.06 m, 1.00 m], S3 [5.07 m, 4.30 m, 1.00 m], S4 [1.34 m, 5.54 m, 1,00 m]. The whole circuit is connected by radio frequency (RF) coaxial cable with matching impedance of 50 Ω. Meanwhile, a partial discharge detector (GDJF-2008) is adopted to inspect the level of discharge during the test. To ensure authenticity and reduce redundancy of extremely huge amounts of data, 2 methods are used for sampling. For phase resolved partial discharge (PRPD) analysis, a peak detector is used in the measurement system to meet the required sampling rate, the statistical data is sampled at a rate of 5 MS/s and the sampling period is every power frequency cycle (20 ms). The sampling rate is 10 GS/s when collecting the specific waveform of the UHF signal, and the sampling period is 1 μs every time. For each PD type, 1000 repeated tests and data are recorded.

IV. PD TEST RESULTS

With regard to the 4 types of PD failures set in bushing, voltage is slowly increased to obtain the values of partial discharge inception voltage (PDIV) and relatively stable discharge activities. Then PRPD spectrum and PD waveforms for each PD type were obtained.

(a) Corona discharge at the top of bushing: The PDIV was determined at 21.73 kV. Ultraviolet (UV) imager was used to record and capture the UV videos of the discharge from outside, as shown in Fig. 5. An obvious corona discharge was seen through UV imaging and the corresponding PRPD spectrum is shown in Fig. 6 (a). The phase distribution of the corona discharge is relatively concentrated, between 0° -100° and 180° -300°. Its amplitude distribution is rarely around 0.0 - 0.1, and it is more evenly distributed between 0.1 – 1.0 of the normalized amplitude.

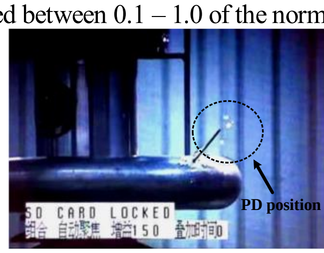

Fig.5 Ultraviolet imaging of corona discharge

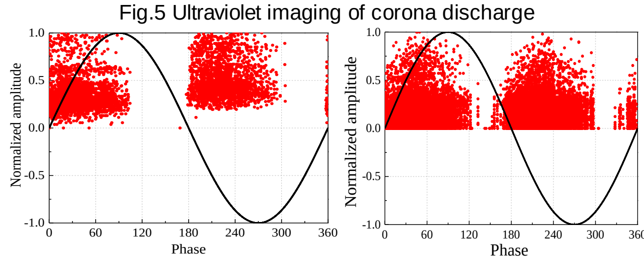

(a) Corona discharge (b) Suspension discharge

Fig.6 PRPD spectrum of corona discharge and suspension discharge

(b) Suspension discharge of electrostatic shield: The PDIV was 49.90 kV for suspension type. The discharge developed rapidly with obvious sound, and the apparent discharge magnitude reached 10412 pC when the voltage was increased to 62.26 kV. The corresponding PRPD spectrum is shown in Fig. 6(b). PDs distribute at 0° - 120°, 160° - 300° and 330° - 360°. The phase distribution range is wide and the top of spectrum is conical shape. After the discharge, there were obvious signs of ablation and blackening at the bottom of the bushing, as shown in Fig. 7, which also proved that the discharge was just caused by suspension discharge of electrostatic shield.

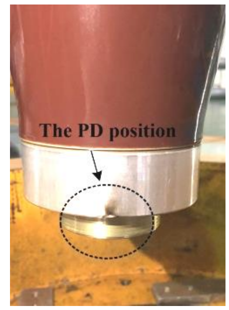

Fig.7 Signs of ablation and blackening by PD

(c) Creeping discharge along the surface of lower porcelain envelope: The PDIV was as low as 11.13 kV and UHF signal was relatively obvious when the voltage was continuously increased around 65.83 kV, then the apparent charge magnitude reached 440 pC. The corresponding PRPD spectrum is shown in Fig. 8(a). There are discharges activities throughout the cycle, mainly distributed at 0° - 120 °, 180° - 300°.

(d) Interior discharge of the bushing: The PDIV was high but it would easily develop to breakdown phenomenon once the PD was generated and accumulated. The apparent charge magnitude increased rapidly when the voltage continued to go up. The overall distribution of the spectrum is trapezoidal and has a high degree of symmetry, distributed at 0° - 120°, 150° - 300°, and 330° - 360°.

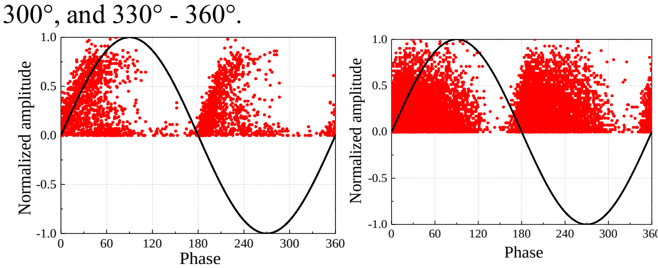

(a) Creeping discharge (b)Interior discharge

Fig.8 PRPD spectrum of creeping discharge and interior discharge

The corona discharge is on the surface of bushing (exposed to the air) and apparent charge amplitude changes obviously as the voltage goes up, the PD events are stable and obvious (more than 500 pC). In contrast, the other 3 defects are immersed in oil, the evolution of PD becomes more difficult. Moreover, the amplitude of the PDs in the oil is more dispersed, the statistical phase distribution is wider and more symmetric. For the 3 types in oil, the positive and negative half-cycles the PRPD spectrum is similar to a "inverted V" shape. PD activities appears at rising and falling edges of sinusoidal voltage, because the applied voltage charges more at the edges. Due to the overlapping between the applied electric field and the field generated by the space charges at voltage polarity reversal, PD phase is biased towards to the voltage zero crossing points.

This article has been accepted for publication in a future issue of this journal, but has not been fully edited. Content may change prior to final publication. Citation information: DOI 10.1109/JSEN.2021.3066809, IEEE Sensors Journal

According to PPRD spectrum distribution, it is clear that the spectrums corresponding to 4 PD types have different characteristics. From the perspective of quantitative analysis, 2 channels of UHF signals (UHF1 and UHF2) are taken to analyze and calculate the skewness *S* and kurtosis *K* of the positive and negative half-cycles of PRPD. The calculation of *K* and *S* are shown as:

$$S = \frac{\sum_{i=1}^{n}(x_i - \bar{x})^3}{n} \tag{1}$$

$$K = \frac{\sum_{i=1}^{n}(x_i - \bar{x})^3}{n\left(\sqrt{\frac{1}{n}\sum_{i=1}^{n}(x_i - \bar{x})^2}\right)^4} \tag{2}$$

x_i is amplitude of each point of PRPD, $\bar{x}$ is average of all points, *n* is the amounts of total points. The obtained *S* and *K* are shown in Fig. 9. The + signature symbol behind represents the skewness of is calculated for the positive cycle while the – symbol represents that of a negative cycle.

The distribution of *S* is relatively concentrated, the varieties corresponding to (b) suspension discharge and (c) creeping discharge are small, but the values of *K* with PD type and power polarity are obvious. In fact, the PD type can be identified by combining the values of *S* and *K* [17]. However, drawing a spectrum requires a large amount of PD data and enough spectrums are necessary to complete the classification of PD faults. To reduce the data dependence and increase the efficiency of calculation, PD waveform features instead of the full waveform are used. Subsequent analysis starts with waveform features instead of statistical spectrums to achieve PD classifications.

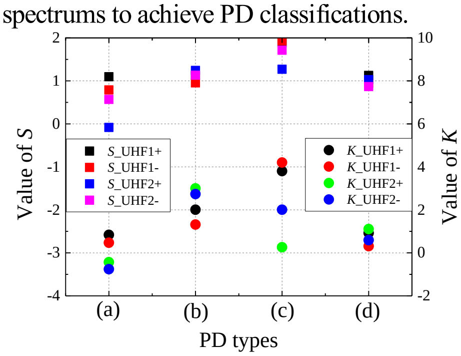

Fig.9 PRPD-based skewness (*S*) and kurtosis (*K*) values of 4 PD faults

V. UHF WAVEFORM FEATURE BASED PD CLASSIFICATION

Due to factors influenced by PD generation, location and medium, different PD types have time-domain and frequency-domain features. It is possible to classify PD defects based on these specific features by referencing PD classification-related work [25]. However, with regard to the distinct structure and propagation law of electromagnetic waves of the bushing, it's necessary to explore the appropriate approach and accurate parameters involved. PD classification based on UHF waveform includes the following 3 steps. Firstly, the UHF waveform is enveloped to reduce redundant information. Then 16 features of the time and frequency domain are extracted and dimensionality is reduced by PCA and ET. Finally, the model is built and PD classification is realized through SVM.

A. Feature extraction for the UHF waveform

Since the UHF frequency band is wide, and it is unavoidable to have interferences during the UHF signals acquisition, the time-domain signals show drastic fluctuations. It is difficult to extract effective features. enveloping the waveform helps to reduce excessive information effectively. Current methods for extracting the envelope include cubic spline interpolation, Hilbert-Huang transform, Gaussian kernel smoothing, etc. [26].

The cubic spline interpolation involves connecting the peak points of the waveform with a smooth curve, which has a continuous 1st and 2nd derivative. But it still keeps a lot of unnecessary information after several times of enveloping. Therefore, Gaussian kernel smoothing is chosen to envelop due to its higher efficiency. The smoothed envelope curve can be obtained by convolving the Gaussian function with the raw waveform. The formula of the Gaussian function is:

$$G(t) = \frac{1}{\sqrt{2\pi}\sigma} e^{-\frac{t^2}{2\sigma^2}} \tag{3}$$

The value of σ controls the shape of the Gaussian function, the smaller the value, the higher and sharper the function. When the function is convolved with waveform, it needs to determine a convolving range which is the width of the smoothing window *W*. It controls the smoothness of the envelope. It is shown that σ=20 , *W*=200 can achieve a proper envelope curve for all of the 4 types of bushing defects. The square of the UHF signal was calculated to obtain a unipolar energy waveform, the two parameters can be obtained as sample waveforms as shown in Fig. 10 (a) - (d).

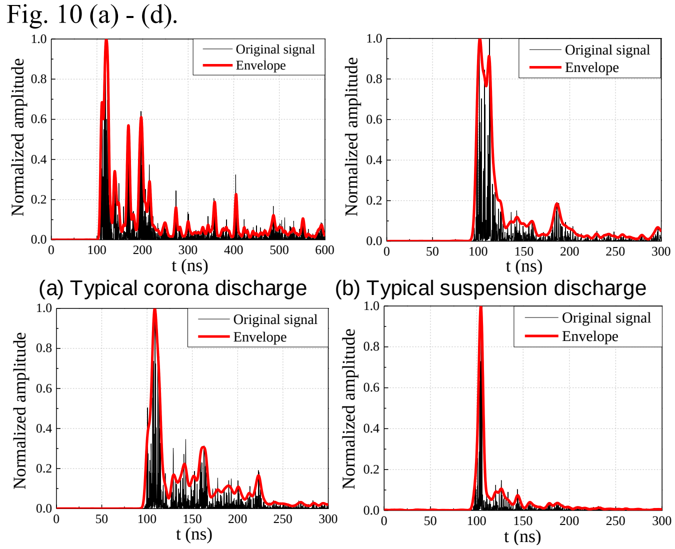

(a) Typical corona discharge (b) Typical suspension discharge

(c) Typical creeping discharge (d) Typical interior discharge

Fig.10 The amplitude of different PD time domain signal and the envelopes

The duration, rise time, fall time and degree of oscillation of each waveform are significantly different, which provides ideas for subsequent waveform feature analysis. 16 features were selected in time and frequency domain. The time domain features include: absolute mean value, root mean square value, variance, rise time, fall time, pulse width, skewness and kurtosis. The frequency domain (UHF band) features include: absolute mean value, root mean square value, variance, absolute maximum value corresponding to amplitude, absolute maximum value corresponding to frequency, spectrum energy, skewness and kurtosis. The definition of some parameters is illustrated in Fig. 11.

The parameters are calculated for each type of enveloping curve and integrate results into a matrix. Then a 2000×16 matrix is obtained for each type of PD waveform and the total data is an 8000×16 matrix (4 types). *f*1 to *f*16 means the 1st to 16th column of the feature matrix that corresponds to the selected order. Due to the huge amount of data, PCA and ET methods are used for feature selection to reduce calculations in classification and diagnosing.

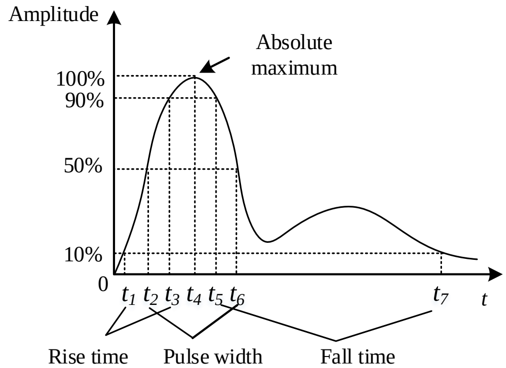

Fig.11 Illustration and calculation of UHF features

The method of PCA is projecting the raw data into a low-dimensional space through orthogonal transformation while retaining the raw data information as much as possible. The matrix composed of the features selected in the previous section has 16 dimensions (16 columns of features). Then the matrix is decentralized and calculated to obtain the corresponding covariance matrix and eigenvalues. The eigenvectors corresponding to the eigenvalues are arranged in descending order. It forms the required transformation matrix to achieve the dimensionality reduction transformation.

Since PCA is actually a basis transformation in a coordinate system, the data sample has the largest variance through the transformation. The column of the new matrix corresponds to the new feature after the transformation of the coordinate system. PCA is used to obtain the corresponding eigenvalue and it is converted into the feature contribution rate as shown in Table I. *F*1 means the 1st column of the new matrix which is transformed from the raw feature matrix by PCA. The first 4 columns of the contribution rate have accumulated to 0.85. Generally speaking, when the principal component contribution rate reaches about 0.85, it can basically reflect the characteristics of the overall data.

TABLE I
RESULTS OF CONTRIBUTION RATE OF COLUMNS OF PCA

Feature	***F*1**	***F*2**	**F3**	***F*4**	***F*5**
Contribution rate	0.58	0.14	0.07	0.06	0.04
Feature	***F*6**	***F*7**	***F*8**	***F*9**	***F*10**
Contribution rate	0.04	0.03	0.02	0.01	0.01

The features are extracted by PCA and arrayed according to contribution rate, then classification is judged from the new matrix. The process eliminates the linear correlation between raw variables and it may ignore nonlinear dependencies. Therefore, ET is used in raw feature extraction to solve this problem. ET is improved on the basis of Random Forest (RF) algorithm. RF contains multiple decision trees trained by random sampling with replacement, finally makes decisions through a majority voting mechanism. ET is based on RF and its improved algorithm. The training data of decision trees selects all the raw data instead of random sampling. When each node in the decision trees selects features, quantitative evaluation criteria in RF are not adopted but are completely randomly selected. Therefore, the generalization ability of the results obtained by ET is actually better.

ET is used for feature selection and the results is shown in Table II. The variance of the spectrum has the highest importance and features in the time domain has greater influence. Although the contribution rate is not like the main components of PCA that are concentrated in the preceding few features and its proportion is low, the information retained is relatively completer and more comprehensive because the training data is raw data without any conversion.

TABLE II
RESULTS OF CONTRIBUTION RATE OF COLUMNS OF ET

Feature	***f*11**	***f*5**	***f*8**	***f*2**	***f*4**
Contribution rate	0.20	0.14	0.09	0.08	0.08
Feature	***f*7**	***f*3**	***f*1**	***f*6**	***f*9**
Contribution rate	0.07	0.07	0.07	0.06	0.03

B. SVM modelling and PD type classification

Because there are a huge number of selected features and it is difficult to divide intuitively, classification is recommended to be performed by means of machine learning. And SVM is adopted to distinguish the 4 bushing PD defects based on UHF information.

SVM is a supervised learning model that analyses data used for classification and regression analysis. It is defined as a linear classifier with the largest interval in the feature space. The learning goal is to find a hyperplane in the *n* dimensional data space to maximize the interval (optimal). Taking a two-dimensional plane as an example, as shown in Figure 12, where *F*1 and *F*5 are selected from Table I. It is difficult to class four types of data on the two-dimensional plane directly. Therefore, we select multiple features and find the optimal hyperplane in the multi-dimensional space to achieve the purpose of accurate segmentation.

Let the optimal hyperplane equation be $f(x) = w^T x + b$, the training samples on both sides correspond to the points that satisfied respectively $f(x)>0$ and $f(x)<0$. Since most of the actual data is not linearly separable, Gaussian kernel formula is adopted due to it is high flexibility to map the raw space of the data into a multi-dimensional space.

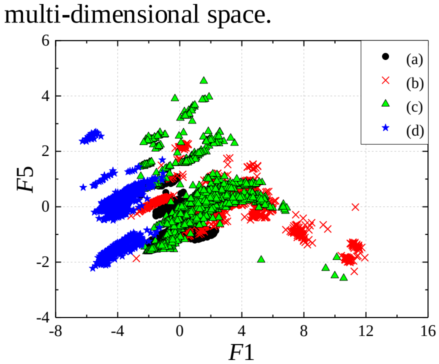

Figure 1. SVM-based classification mapping of bushing faults with F1&F5

In order to improve the fault tolerance of the trained model, we consider the differences in the measurement and transmission of signal. For each PD type, 80% (1600 groups) data is selected randomly as the training set, and the other 20% (400 groups) is used as the test set. Therefore, the test set contains 6400 sets of data (4 PD types). To ensure the accuracy of the trained model, it is verified by 10-fold cross-validation.

The selected features obtained by PCA and ET are input one by one into the SVM for training, then the remaining data is input into the completed training model for classification. The relationship between number of features and diagnosing accuracy is shown as Figure 13.

For the (a) (b) (c) type, the initial recognition accuracy is relatively lower when the number of features used less than 3. As the number of input features increases, the accuracy of 4 PD types could reach 99%, which shows that the features selected actually have good representativeness.

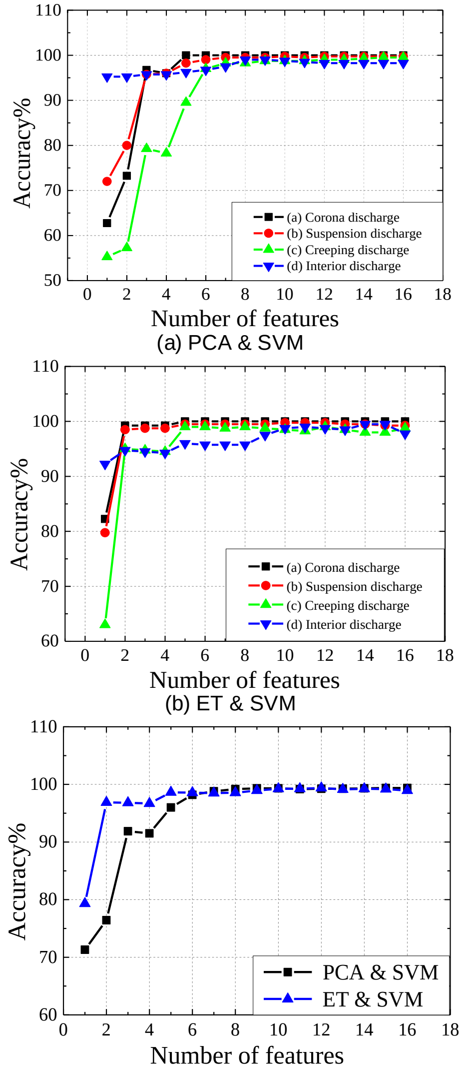

(c) The total accuracy comparison of PCA&SVM and ET&SVM

Figure 2. Relationship between number of features and classification accuracy of 4 PD types

As a comparison, the accuracy reaches 96% when 5 features are included, whereas for the ET method the accuracy reached 96% when 2 features are input. For the same prediction classification accuracy, the training data used by ET is only 40% of PCA. It indicates that the raw feature contains more complete information, which means it needs less data for classification to reach a high accuracy. Moreover, due to less data needs to be processed, it is able to reduce the time required.

VI. Conclusion

In this paper, 110 kV OIP bushing is taken as the research objective and PD feature selection and diagnosis algorithm are proposed with UHF method. The work provides an effective solution for PD detection and diagnosis for OIP bushing in power transformers.

1) UHF technique is investigated as effective approach to detect PD activities inside and outside bushings. Oil gaps between the flange and condenser body in a typical OIP bushing provides an available approach to trace the PD-induced EM signal, then PD activities in a bushing can be detected in a non-destructive way.

2) Feature selection helps to analyze UHF PD signal and provides effective information to subsequent classification. Totally, 16 features in time and frequency domain are considered. Then extraction and dimensionality reduction are performed and compared by PCA and ET, in which ET algorithm has a better performance.

3) Typical defect diagnosis is of great significance for bushing maintenance and evaluation since the ignorance on the bushing detection to date, a combined algorithm with ET and SVM reaches 96% under 2 selected features.

Acknowledgment

The authors thank Xinquan Wang and Bin Feng from Nanjing Zhida Electric Co., Ltd. for their support on the experimental setup and Dr. Qingwei Zhu from The University of Manchester, UK for the discussion on the work.

References

[1] G. M. Ma, et al. "Distributed partial discharge detection in a power transformer based on phase-shifted FBG." *IEEE Sensors Journal*, vol. 18, no. 7, pp: 2788-2795, Apr. 2018.

[2] International Council on Large Electric systems. "Power transformers and reactors – Transformer bushing reliability," *CIGRE*, pp.15-16, Feb. 2019.

[3] S. Ning, Y. He, A. Farhan, Y. Wu and J. Tong, "A Method for the Localization of Partial Discharge Sources in Transformers Using TDOA and Truncated Singular Value Decomposition," *IEEE Sensors Journal*, doi: 10.1109/JSEN.2020.3037699, Nov. 2020.

[4] R. Nikjoo, N. Taylor and H. Edin, "Dielectric response measurement by impulse stimulus on AC: Measurement considerations, and laboratory testing on a bushing," *IEEE Transactions on Dielectrics and Electrical Insulation*, vol. 24, no. 1, pp. 511-518, Feb. 2017.

[5] B. Qi, Q. Dai, C. Li, Z. Zeng, M. Fu, and R. Zhuo, "The mechanism and diagnosis of insulation deterioration caused by moisture ingress into oil-impregnated paper bushing," *Energies*, vol. 11, no. 6, pp. 1496-1508, Jun. 2018.

[6] D. Cahue-Diaz, S. Maximov, R. Escarela-Perez, J. Olivares-Galvan, J. Alvarez-Ramirez, "Computation of temperature distributions in transformer covers due to high crossing currents in bushing regions," *International Journal of Electrical Power & Energy Systems*, vol. 113, pp: 699-712, Dec. 2019.

[7] R. Liao, Y. Du, L. Yang and J. Gao, "Quantitative diagnosis of moisture content in oil-paper condenser bushing insulation based on frequency domain spectroscopy and polarisation and depolarisation current," *IET Generation, Transmission & Distribution*, vol. 11, no. 6, pp. 1420-1426, Apr. 2017.

[8] Z. Xu, et al., "Study on frequency domain dielectric spectroscopy of epoxy resin impregnated paper bushings under damp conditions." *The Journal of Engineering*, vol. 2019, no. 16, pp. 1319-1323, Mar. 2019.

[9] D. Wang, L. Zhou, H. Li, W. Liao, X. Xu and L. Guo, "Moisture estimation for oil-immersed bushing based on FDS method: at a reference temperature," *IET Generation, Transmission & Distribution*, vol. 12, no. 10, pp. 2480-2486, May. 2018.

[10] S. Jan; Mrozik, M. Andrzej, P. Bohatyrewicz, and Z. Marek, "Condition Assessment of HV Bushings with Solid Insulation based on the SVM and the FDS Methods," *Energies*, vol. 13, no. 4, pp. 853-866, Feb, 2020.

[11] J. Jiang, R. Chen, M. Chen, W. Wang and C. Zhang, "Dynamic fault prediction of power transformers based on hidden Markov model of dissolved gases analysis," *IEEE Transactions on Power Delivery*, vol. 34, no. 4, pp. 1393-1400, Aug. 2019.

This article has been accepted for publication in a future issue of this journal, but has not been fully edited. Content may change prior to final publication. Citation information: DOI 10.1109/JSEN.2021.3066809, IEEE Sensors Journal

[12] G. Zhang, et al., "On-Line monitoring of partial discharge of less-oil immersed electric equipment based on pressure and UHF," *IEEE Access*, vol. 7, pp. 11178-11186, Jan. 2019.

[13] L. Zhang et al., "Development of multi-parameter online monitoring equipment for EHV transformer bushing," *IET Science, Measurement & Technology*, vol. 14, no. 1, pp. 98-103, Jan. 2020.

[14] M. Koch and M. Krüger, "A new method for on-line monitoring of bushings and partial discharges of power transformers," *2012 IEEE International Conference on Condition Monitoring and Diagnosis*, pp. 1205-1208, 2012.

[15] M. Botelho, T. Gomes, F. Nazaré, J. Neto, M. Werneck and R. Filho, "A novel monitoring method for condensive bushings," *2013 IEEE International Instrumentation and Measurement Technology Conference*, pp. 1266-1271, 2013.

[16] L. Duan, J. Hu, G. Zhao, K. Chen, J. He and S. X. Wang, "Identification of partial discharge defects based on deep learning method," *IEEE Transactions on Power Delivery*, vol. 34, no. 4, pp. 1557-1568, Aug. 2019.

[17] M. Zhu, Y. Wang, D. Chang, G. Zhang, X. Tong, and L. Ruan, "Quantitative comparison of partial discharge localization algorithms using time difference of arrival measurement in substation," *International Journal of Electrical Power & Energy Systems*, vol. 104, pp. 10-20. Jan. 2018.

[18] F. Yang, G. Sheng, Y. Xu, H. Hou, Y. Qian and X. Jiang, "Partial discharge pattern recognition of XLPE cables at DC voltage based on the compressed sensing theory," *IEEE Transactions on Dielectrics and Electrical Insulation*, vol. 24, no. 5, pp. 2977-2985, Oct. 2017.

[19] X. Peng, *et al*., "A convolutional neural network-based deep learning methodology for recognition of partial discharge patterns from high-voltage cables," *IEEE Transactions on Power Delivery*, vol. 34, no. 4, pp. 1460-1469, Aug. 2019.

[20] A. Ishak, M. Ishak, M. Jusoh, S. Dardin and M. Judd, "Design and optimization of UHF partial discharge sensors using FDTD modeling," *IEEE Sensors Journal*, vol. 17, no. 1, pp. 127-133, Jan. 2017.

[21] X. Han, J. Li, L. Zhang and Z. Liu, "Partial discharge characteristics of metallic protrusion in GIS under different lightning impulse voltage waveforms based on UHF method," *IEEE Transactions on Dielectrics and Electrical Insulation*, vol. 24, no. 6, pp. 3722-3729, Dec. 2017.

[22] Melazzi D., Lancellotti V. and Capobianco A.D., "Analytical and numerical study of a gaseous plasma dipole in the UHF frequency band," *IEEE Transactions on Antennas and Propagation*, vol. 65, no. 12, pp. 7091-7101, Dec. 2017.

[23] J. Jiang, K. Wang, C. Zhang, M. Chen, H. Zheng and A. Ricardo, "Improving the error of time differences of arrival on partial discharges measurement in gas-insulated switchgear," *Sensors*, vol. 18, no. 11, pp. 4078-4089, Nov, 2018.

[24] J. Li, P. Wang, T. Jiang, L. Bao and Z. He, "UHF Stacked Hilbert Antenna Array for Partial Discharge Detection," *IEEE Transactions on Antennas and Propagation*, vol. 61, no. 11, pp. 5798-5801, Nov. 2013.

[25] X. Peng et al., "A Convolutional Neural Network-Based Deep Learning Methodology for Recognition of Partial Discharge Patterns from High-Voltage Cables," *IEEE Transactions on Power Delivery*, vol. 34, no. 4, pp. 1460-1469, Aug. 2019.

[26] M. Zhu et al., "Discrimination of three or more partial discharge sources by multi-step clustering of cumulative energy feature es," *IET Science, Measurement & Technology*, vol. 13, no. 2, pp. 149-159, Mar. 2019.

Jun Jiang (SM'20, M'14) was born in Anqing, China, in 1988. He received the B.E. degree in electrical engineering and automation from China Agricultural University (CAU) in 2011 and PhD degree in high voltage and electrical insulation from North China Electric Power University (NCEPU) in 2016. In 2019-2020, he worked as academic visitor (Honorary Stuff) in Department of Electrical & Electronic Engineering, School of Engineering, The University of Manchester, UK.

He is now working as an Associate Professor in Center for more-electric-aircraft power system, Nanjing University of Aeronautics and Astronautics, Nanjing 211106, China. His research interests are advanced sensing techniques and their application in condition monitoring of power apparatus.

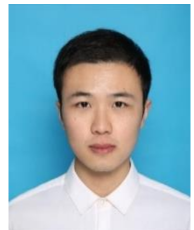

Judong Chen (S'20) was born in Yichun, Jiangxi, China, in 1996. He received the B.E. degree in Huazhong University of Science and Technology (HUST) in 2018 and M.S degree in Nanjing University of Aeronautics and Astronautics (NUAA) in 2021. He is now working in State Grid Jiangxi Maintenance Company, Jiangxi, 330000, China.

Yifan Bie (S'20) was born in Qianjiang, Hubei, China, in 1996. He received te B.E degree in Chongqing University (CQU), China, in 2017.

He is currently pursuing the Master degree in Department of Electric Engineering, Nanjing University of Aeronautics and Astronautics (NUAA). His research interests are condition monitoring of power apparatus, especially in the field of bushings.

Prem Ranjan (S'19, M'20) was born in Bihar, India, in 1994. He obtained the B.Tech. degree in Electrical and Electronics Engineering from NIT Calicut in 2015 and MS, PhD degrees in Electrical Engineering from IIT Madras, India in 2019. He is currently working as a postdoc researcher at Department of Electrical & Electronic Engineering, The University of Manchester, UK. His current research interest includes exploding wire and condition monitoring of power apparatus.

Chaohai ZHANG was born in Nanjing, China, in 1963. He obtained his B.A., M.S. and Ph.D. degrees from Harbin Institute of Technology (HIT), Navy Aeronautical Engineering Academy (NAEA) and Hong Kong Polytechnic University (HKPU), respectively. After some years' experiences of research working as a JSPS Research Fellow in Japan and as a research engineer in Canada, respectively, currently he is a Professor at Nanjing University of Aeronautics and Astronautics (NUAA), Nanjing, China. His research interests are in electrical discharges, plasma, electrical environment and condition monitoring and diagnosis of electric power equipment.

Harald SCHWARZ graduated as master of science in electrical engineering from Berlin University of Technology in 1982 and got his Ph.D. degree in electrical engineering from the University of Dortmund in 1986. From 1987 till 1995, he worked with ASEA BROWN BOVERI (ABB) in large power transformers and high voltage switchgears before he joined Brandenburg University of Technology (BTU) in Cottbus as a full professor in energy distribution and high voltage engineering. In 1999, he commissioned one of the largest high voltage test fields at German universities. From 2002 to 2004, he was vice dean of Faculty for Mechanical, Electrical and Industrial Engineering and from 2004 to 2014, he was managing director of CEBra—Center for Energy Technology Brandenburg at BTU Cottbus, a central scientific research center under direct responsibility of the university president. In 2014, he established the Power System Simulation Center, which is unique at German university. Based on the university central campus with its peak load of 2.5 MW, he actually built up a smart grid with battery, heat and gas storages, renewable and conventional generation, as well as flexible loads from power-to-gas, to-heat and to-vehicle. In 2015, he was honored the professor of "Peter the Great" by St. Petersburg University of Technology and from Oct. 2013 to end of 2014, he was a senator of the enlarged founding senate of BTU Cottbus-Senftenberg.